On the Edge Refraction Contrast Imaging on a Conventional Neutron Diffractometer Employing Dispersive Double-Crystal Monochromator

P Mikula[1], M Vrána[1], V Em[2], J Čapek[3] and D Korytár[4]

[1]Nuclear Physics Institute ASCR, v.v.i., 25068 Řež, Czech Republic
[2]National Research Centre "Kurchatov Institute", Moscow, 123182, Russia
[3]Faculty of Math. and Physics, Charles University, Prague, Czech Republic
[4]Institue of Physics SAS, Dúbravská cesta 9, 845 11 Bratislava, Slovak Republic

E-mail: mikula@ujf.cas.cz

Abstract. Conventional radiography is based on absorption effects, which depend only on the imaginary part of the refractive index. However, slits and macroscopic objects such as edges give rise to refraction and this phenomenon can be effectively used in the so called phase-contrast imaging. In addition to the absorption contrast in the conventional radiography, it exploits also contributions of phase shifts induced by the propagation of a coherent neutron (or X-ray) beam through an investigated sample. The difference in real part of the refrative index between a studied detail and its vicinity results in a phase shift between the wave transmitted through and outside the detail. Due to this phase shift, the two waves interfere. However, the used radiation has to possess a sufficiently high spatial coherence permitting one to detect resulting interference pattern. In this contribution we present two simple neutron diffractometer configurations based on two bent perfect Si crystals which provide a high spatial coherence beam of sufficient intensity which could be potentially used in some phase contrast radiography experiments.

1. Introduction

It is well known that depending on geometry or performance of diffraction by single crystals one can easily manipulate e.g. with resolution, cross-section and focusing properties of the diffracted beam in the scattering plane. In the case of manipulation of the cross-section of the beam, the simplest way is to use asymmetric diffraction geometry, which has been studied many times and described in many text books related to neutron or X-ray diffraction. Namely, it is often used for special monochromator systems on scattering instruments using synchrotron radiation. The extreme case of the asymmetric diffraction geometry is so called fully asymmetric diffraction geometry (FAD geometry). Such a unique diffraction geometry employing crystal of large dimensions, namely the length, is practically applicable only in neutron diffraction. Neutron has a high penetration ability and bent perfect crystals (BPC) of Si are very suitable for such experiments and studies. For observation and imaging of edge

[1] To whom any correspondence should be addressed.

refraction effects one needs to have not only a beam of a sufficiently large cross-section but also the beam has to have a required spatial coherence [1-7]. High coherence of the beam, however, can be easily achieved by using a dispersive or quasi-dispersive double-crystal diffraction setting employing optimally bent perfect crystals (see figures 1 and 2). In the case of using the FAD geometry, two alternatives can be distinguished: the FAD geometry with the output beam compression and the opposite one - the FAD geometry with the output beam expansion. In the former case e.g. a wide incident polychromatic beam is impinging the crystal and a narrow (compressed) beam is diffracted when passing the crystal perpendicularly to its thickness e.g. along its longest edge. Of course, such alternative is not suitable for studies of edge refraction effects. This alternative was already tested in the eighties for exploitation in the designing of new types of neutron monochromators [9-10]. In the latter case a narrow beam enters the bent-crystal slab through the end face and, after passing along the longest edge of the slab, the diffracted monochromated beam is expanded to a large cross-section (see figure 2). Such FAD geometry has been then succesfully employed in the high resolution double bent crystal (1,-1) SANS diffractometer with the FAD analyzer as a second crystal [11-17] which provided

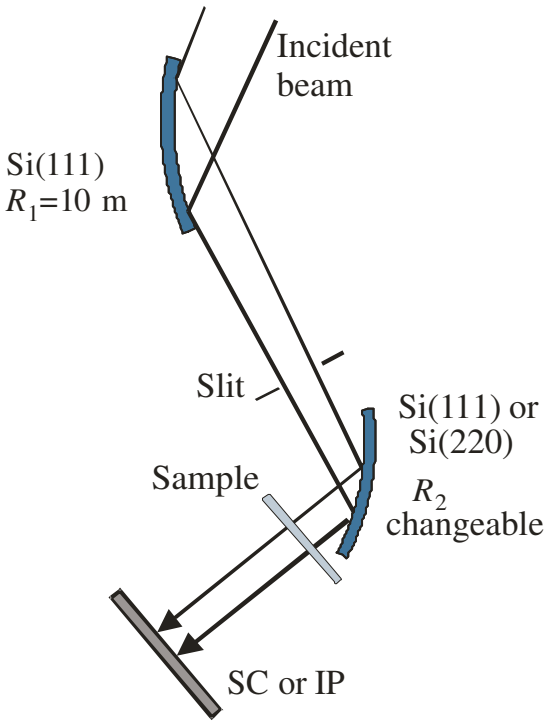

Figure 1. Scheme of the quasi-dispersive diffractometer performance. SC - scintillation camera, IP - imaging plate.

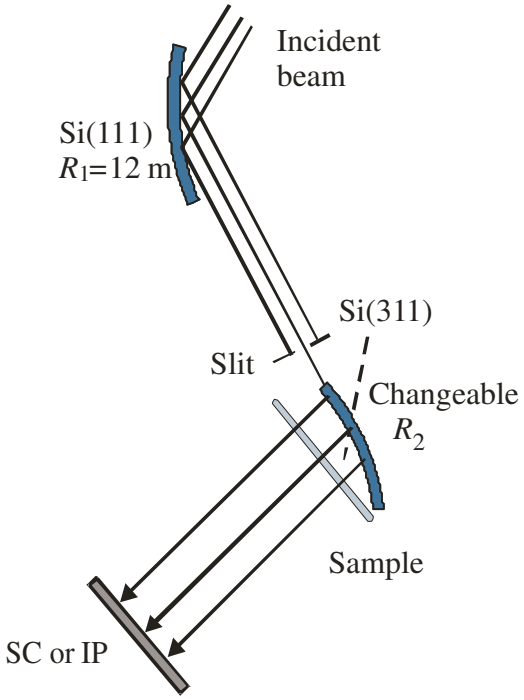

Figure 2. Scheme of the quasi-dispersive diffractometer performance with the BPC Si(311) crystal in FAD geometry.

a substantial enlargement of the range of analyzed angles that could be transformed to a linear spatial dimension. It opened the possibility to use a one dimensional position sensitive detector for the analysis of the SANS signal instead of the step-by-step analysis with the conventional symmetric diffraction geometry of the crystal analyzer. Recently, double bent crystal dispersive (n,-m) arrangement with the second FAD crystal in the the output beam expansion diffraction geometry has been studied for the imaging of edge refraction effects [10,11] by using rather complicated three axis diffractometer setting. In this case, before the double-crystal system a bent perfect premonochromator was used. In the present paper we introduce simpler versions providing monochromatic beams of acceptable spacial coherence permitting to observe edge refraction effects.

2. Experimental details

The experiments were carried out on the neutron optics diffractometer operating at λ=0.162 nm which is installed at the medium power research reactor LWR-15 in Řež. Figures 1 and 2 show schematically

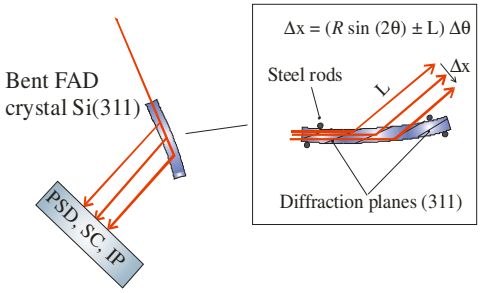

Figure 3. The detail of the FAD geometry transforming an angular deviation $\Delta\theta$ from the mean Bragg position.

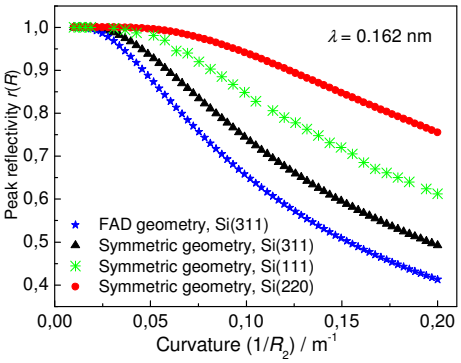

Figure 4. Peak reflectivity vs crystal curvature for several crystal slabs.

the double bent crystal arrangements. Figure 3 shows the detail of the FAD diffraction transforming an angular deviation $\Delta\theta$ from the mean Bragg position, e.g. in the middle of the FAD-crystal, to the linear spatial shift Δx [12]. In combination with the dispersive setting with the bent Si(111) crystal such double crystal configuration represents a self-collimation system providing a high spatial coherence without necessity to use any Soller collimator. For bending the BPC slabs we used four-point bending devices [16] (see the steel rods in figure 3). The reflecting properties of the BPC slabs will not be discussed here and can be found in our second paper of these proceedings or in detail in [8]. Here we introduce only the reflection probability (called peak reflectivity) of the neutron when meeting the Bragg condition in the BPC Si-crystal as a function of the crystal curvature. The dependences for Si(311) reflection with the crystal in symmetric and FAD diffraction geometries are shown in figure 4 for the sake of comparison. All Si crystal slabs used in the experiment were of the length of 200 mm and the width (height) of 40 mm. The thickness of the first Si(111) slab working as a monochromator was 4 mm. It had a fixed curvature of 0.08 nm^{-1} (R_1=12 m). As a second crystal we used successively Si(111), Si(220) and FAD-Si(311) of the thickness of 2 mm, 3 mm and 4 mm, respectively. For the imaging of the beam profiles from the second crystal (without a sample) we used scintillation camera (SC) of the spatial resolution of 0.1 mm and for imaging of the edge profiles of the beam after passing through the sample we used the Imaging plate (IP) having 50 μm spatial resolution.

3. (1,-1) diffraction setting with the 2 mm thick Si(111) second slab (see figure 1)

First, as a second crystal we used the bent Si(111) crystal in the (1,-1) setting. However, due to the opposite sense of the curvatures of the individual slabs, the setting is slightly dispersive. As

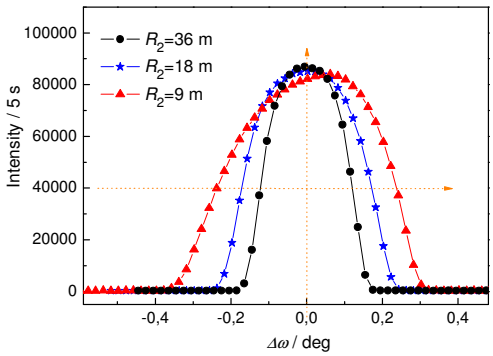

Figure 5. Rocking curves (RC) of the second Si(111) bent perfect crystal for different R_2.

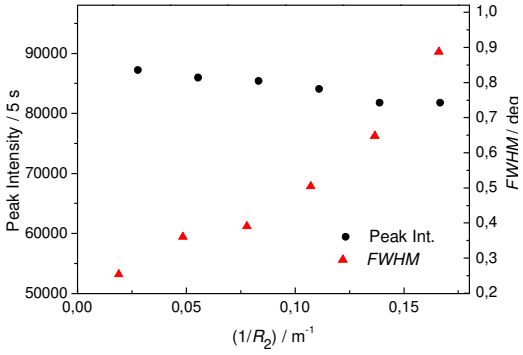

Figure 6. Parameters of the rocking curves vs the curvature of the second Si(111) slab.

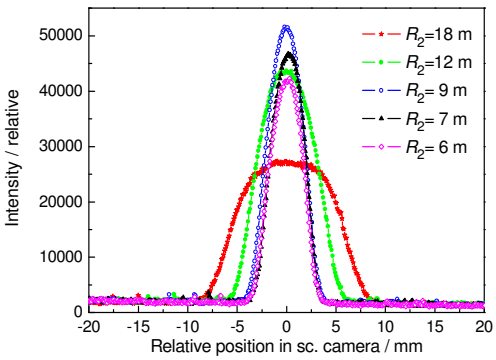

Figure 7. Diffraction profiles of the output beam taken at the peak of the rocking curve and imaged by SC at the distance of 65 cm.

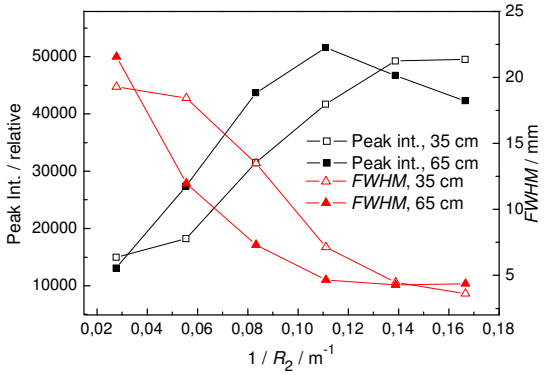

Figure 8. Parameters of the diffraction profiles registered by SC at 35 cm and 65 cm.

documented in the figures from 5 to 8, the dispersity becomes stronger with the increase of the crystal curvature. On the other hand, when the crystals have the curvatures of the same sense, the setting becomes nearly nondispersive depending on the mutual distance of the bent crystal slabs (for details we refer to [8], [9] and [12]). The figures from 9 to 11 show that a slight dispersity of the setting provides a sufficient spatial coherence required for observation of the edge refraction effects.

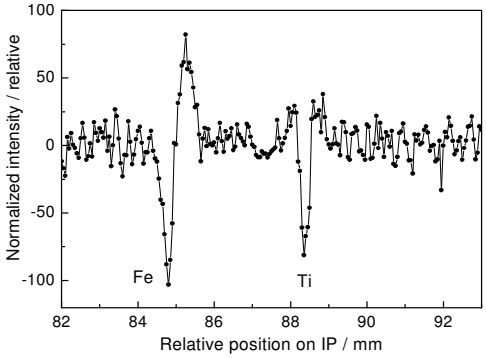

Figure 9. Refraction effects obtained on Fe (2 mm) and Ti (2 mm) edges for IP at 40 cm from the sample and R_2=36 m.

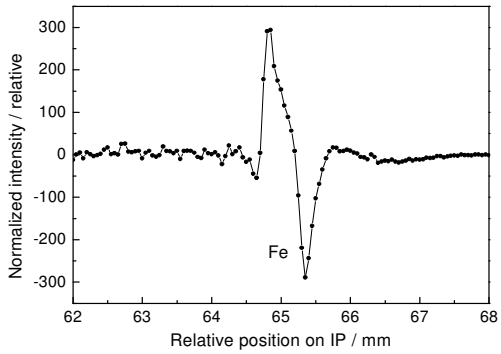

Figure 10. Refraction efffect on Fe (9 mm) edge for IP at 35 cm from the sample and R_2=36 m.

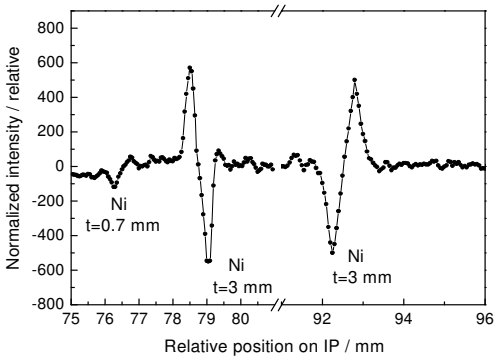

Figure 11. Refraction effects obtained on edges of Ni plates of different thickness t for IP at 40 cm and R_2=36 m.

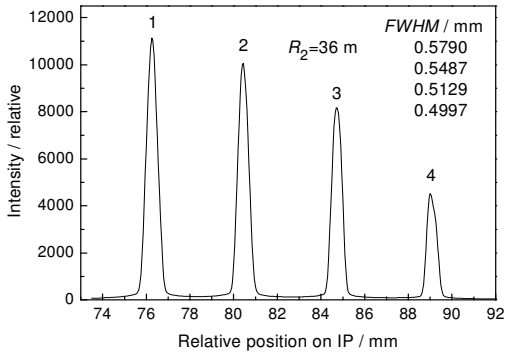

Figure 12. *FWHM*s of the profiles of the beam passing through Gd slits of different widths (see text) at the distance of 40 cm.

Figure 12 shows the collimation of the double diffracted beam when using a system of Gd slits of the width of 0.47 mm, 0.36 mm, 0.24 mm and 0.11 mm. The beam divergence was of about 1x10^{-3} rad.

4. (n,-m) diffraction setting with the 3 mm thick Si(220) second slab (see figure 1)

Similarly to the previous setting, in this case we used a Si(220 slab as a second crystal which makes together with the Si(111) monochromator quasi-dispersive perfomance. The inspection of the figures

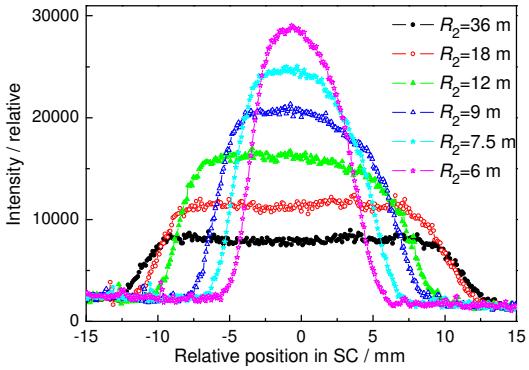

Figure 13. Diffraction profiles of the output beam taken at the peak of the rocking curve and imaged by SC at the distance of 35 cm.

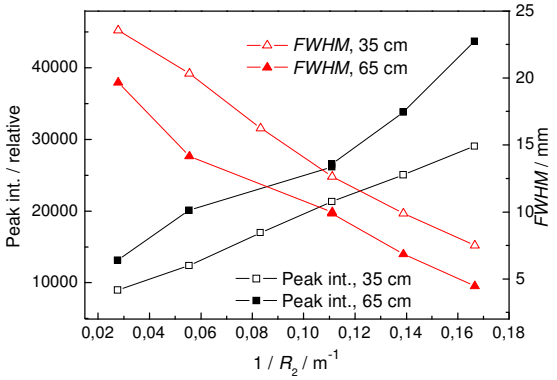

Figure 14. Parameters of the diffraction profiles registered by SC at 35 cm and 65 cm.

13 and 14 reveals that with the increase of the curvature $1/R_2$, the dispersity of the setting becomes more pronounced and thus the *FWHM* of the beam profile decreases. However, the peak intensity of

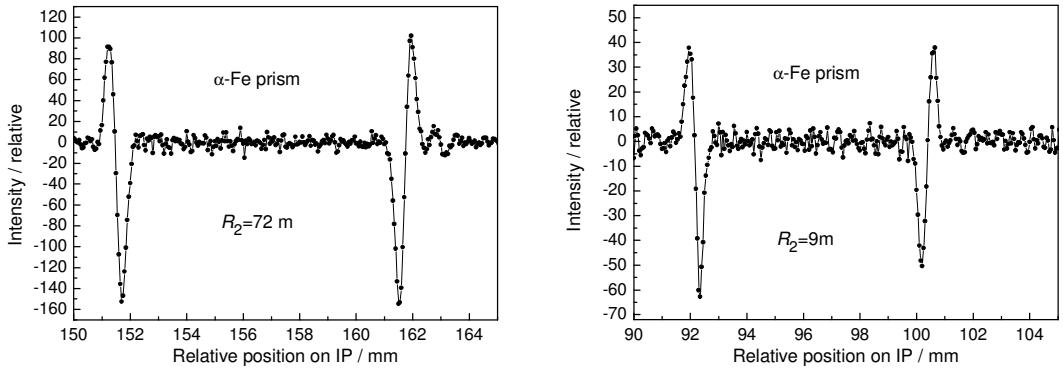

Figure 15. Refraction effects on both sides of squared 9 mm α-Fe prism imaged by IP at 40 cm from the sample and for R_2=72 m and R_2=9 m.

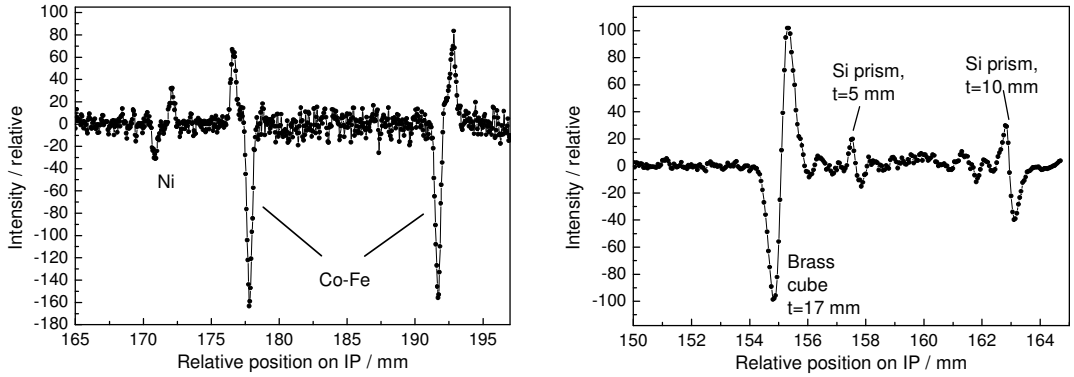

Figure 16. Refraction effects on both sides of Co-Fe plate and a Ni of 3 mm imaged by IP at 32 cm from the sample and for R_2=12.5 m.

Figure 17. Refraction effects on three samples of different widths t of edges imaged by IP at 40 cm from the sample and for R_2=9 m.

the profile increases due to the increase of the effective mosaicity of the BPC slab. In the whole range of curvatures the focusing is rather weak (see the difference in *FWHM* for the distance of 35 cm and 65 cm). Figures from 15 to 17 show several examples of the imaging of the edge refraction effects and document the quality of the output double diffracted beam.

5. (n,-m) diffractometer setting with the BPC Si(311) crystal in the FAD geometry

As a most promisig configuration, the (n,-m) diffractometer setting with the BPC Si(311) crystal in the FAD geometry has appeared. Of course, depending on the crystal cut of the slab one can use the FAD diffraction geometry with another system of lattice planes. By using the Si(311) reflection the dispersity of the (n,-m) is more pronounced than in the previous case. In addition, depending on the curvature of the FAD crystal the width of the double diffracted beam could be substantially enlarged as demostrated in the next figure 18. Such a large beam was then used for the imaging of the teeths of a 8 cm wide steel comb. One part of the result can be seen in figure 19. The next figures from 20 to 23 provide further examples of refraction effects on the edges of different materials.

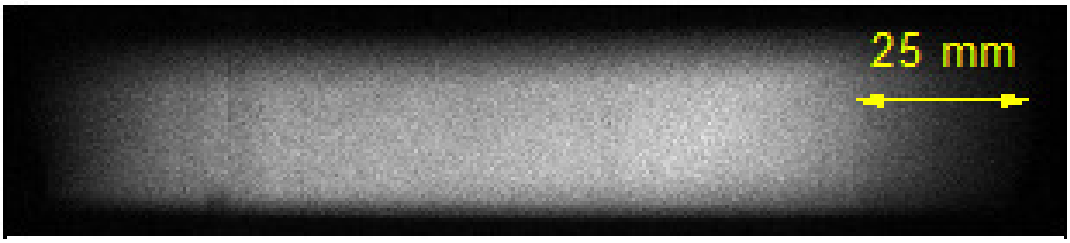

Figure 18. An example of the image of the diffracted beam by the FAD crystal for $R_{2,FAD}$=12 m.

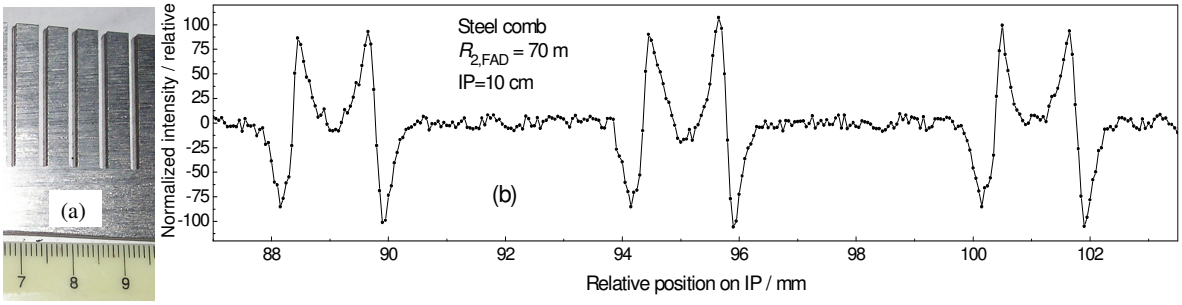

Figure 19. Imaging of the refraction effects (b) on the steel comb (a) with 4.5x4.5 mm^2 teeth.

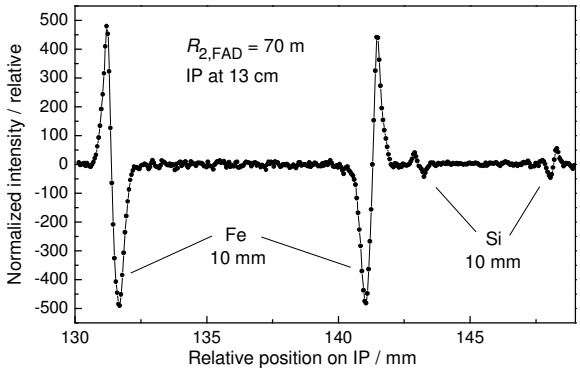

Figure 20. Refraction effects on the edges of squared α-Fe (10 mm) and Si (10 mm) samples.

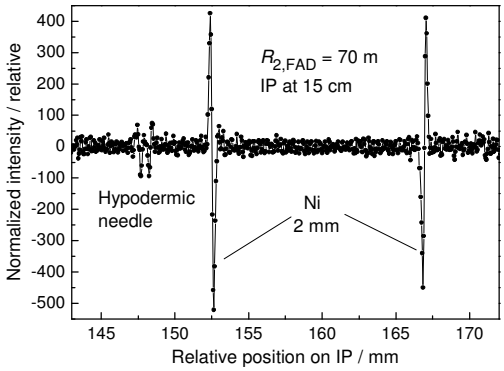

Figure 21. Refraction effects on a hypodermic needle and Ni (2 mm) edges.

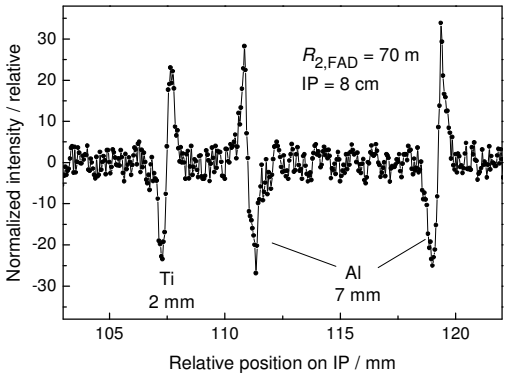

Figure 22. Refraction effects on the edges of Ti (2 mm) and Al (7 mm) samples.

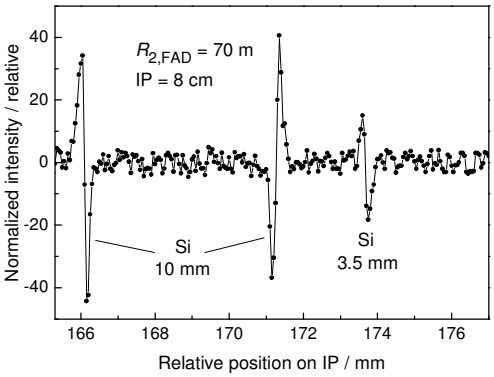

Figure 23. Refraction effects on the edges of Si (10 mm) and Si (3.5 mm) samples.

6. Summary

The quasi-dispersive double bent crystal arrangements provide a highly parallel monochromatic beam having a cross-section of several square centimetres which can be also suitable, besides other things, for conventional radiography experiments. Moreover, the beam possesses sufficiently high spatial coherence and thus, the phase shift contrast phenomenon can be also exploited. As can be seen from the presented figures, the refraction edge profiles can be observed even in the (1,-1) setting of the bent Si(111) crystals with the mutual curvatures far from the nondispersive diffraction geometry. However, it should be pointed out that the quasi-dispersive experimental performances have such excellent properties only in one dimension, i.e. in the scattering plane. As demonstrated in the FAD case, the spatial coherence and the magnifying of the beam cross-section can be (in some range) easily manipulated by changing the curvature of the FAD crystal.

Acknowledgements

The related measurements were carried out at the CANAM infrastructure of the NPI ASCR Rez. Bragg diffraction optics investigations are in the Czech Republic supported by GACR project no. 14-36566G, by the ESS project LM2010011: 'Contribution to Partnership in Large Research Infrastructure of Pan-European Importance' as well as by the project of EU-FP7-NMI3 II: "Integrated Infrastructure Initiative for Neutron Scattering and Muon Spectroscopy", 2009-2015.

References

[1] Podurets K M, Somenkov E A, Chistyakov R R and Shilstein S Sh 1989 *Physica B: Condensed Matter*, **156-157** 694-697.
[2] Treimer W and Schaper J 1996 *BENSC Experimental Report*, p 321.
[3] Treimer W, Feye-Treimer U and Herzig C 1998 *Physica B* **241-243** 1197-1203.
[4] Kardjilov N, Lehmann E, Steichele E and Vontobel P 2004 *Nucl. Instrum. Methods in Phys. Res.* **A 527** 519-530.
[5] Strobl M, Treimer W, Kardjilov N and Hilger A 2005 *Nucl. Instrum. Methods in Phys. Res.* **A 542** Issues 1-3, 383-386.
[6] Strobl M, Treimer W, Kardjilov N, Hilger A and Zabler S 2008 *Nucl. Instrum. Methods in Phys. Res.* **B 266** 181-186.
[7] Strobl M, Kardjilov N, Hilger A, Kune G, Frei G and Manke I 2009 *Nucl. Instrum. Methods in Phys. Res.* **A 604** 640-645.
[8] Mikula P, Kulda J, Vrána M and Chalupa B 1984 *J. Appl. Cryst.* **17** 189-195.
[9] Mikula P, Chalupa B, Kulda J, Vrána M, Sedláková L and Michalec R 1985 *J. Appl. Cryst.* **18** 135-140.
[10] Mikula P, Kulda J, Horalík L, Chalupa B and Lukáš P 1986 *J. Appl. Cryst.* **91** 324-330.

[11] Lukáš P, Mikula P, Šaroun J and Strunz P 1994 *Nucl. Instrum. Methods in Phys. Research*, **A 338** 111-115.
[12] Šaroun J, Lukáš P, Mikula P and Alefeld B 1994 *J. Appl. Cryst*. **27** 80-88.
[13] Hempel A, Eichhorn F, Reichel P and Boede W 1996 *Nucl. Instrum. Methods in Phys. Res*. **A 381** 466-471.
[14] Mikula P, Vrána M, Seong B S, Woo W, Em V and Korytár D 2014 *IOP Publishing Journal of Physics: Conference Series*, **528** 012004.
[15] Mikula P, Vrána M, Šaroun J, Pilch J, Seong B S, Woo W and Em V 2014 *J. Appl. Cryst*. **47** Part 2, 599-605.
[16] Mikula P, Kulda J, Lukáš P, Vrána M, Ono M and Sawano J 2000 *Physica B*, **276-278** 174-176.